Fabrication and characterization of a pulsed fiber ring laser based on As_2S_3

Thibault North* and Martin Rochette

McGill University, Department of Electrical and Computer Engineering, Montréal (Québec), H3A 2A7, Canada
**Corresponding author: thibault.north@mail.mcgill.ca*

Received October 27, 2011; revised January 10, 2012; accepted January 12, 2012;
posted January 12, 2012 (Doc. ID 157112); published February 14, 2012

We demonstrate the operation of a fiber ring laser using a 19.5 cm segment of As_2S_3 chalcogenide fiber. The laser is passively mode-locked via nonlinear polarization rotation and provides two different operation regimes of picosecond and noiselike pulses. This ring configuration also enables an accurate measurement of the chromatic dispersion of the chalcogenide fiber. © 2012 Optical Society of America

OCIS codes: 060.3510, 140.0140, 140.3510, 190.0190, 190.4370, 320.5390.

Fiber ring lasers are known to produce short and powerful pulses, for example, when passively mode-locked using nonlinear polarization rotation (NPR) [1] or saturable absorbers [2]. In the particular case of NPR, the combined effects of cross-phase modulation (XPM) and self-phase modulation (SPM) lead to a nonuniform rotation of the polarization state across the pulse. As a consequence, the combined effect of NPR and a polarizer shortens pulses at every cavity round-trip by transmitting their highest intensity components and attenuating their wings [3]. It has been shown that the total dispersion in an NPR-based ring dictates the minimum achievable pulse width [4], and pulses as short as 77 fs have been demonstrated in a dispersion-compensated fiber cavity [5]. In order to avoid the deterioration of pulses and stability issues, the nonlinear phase shift the pulse experiences must remain under a maximum of 2π [6,7]. However, when it is not the case, noiselike pulses will propagate in the cavity [8].

Previous reports of mode-locked fiber lasers using chalcogenide fiber include only one paper, a chalcogenide fiber ring laser where chalcogenide serves as a host for neodymium. It has a self-pulsing behavior at 1080 nm with 0.2 μs pulses, whose origins are related to a saturable-absorption effect in the doped fiber [9]. In this paper, we make a first demonstration of using chalcogenide glass as the nonlinear medium for self-pulsation in a fiber ring laser. The high nonlinearity provided by the chalcogenide glass enables the formation of pulses at low peak power. This is very valuable in designs with a gain medium of low saturation power, which occurs when compactness is a primary requirement. In addition to its high nonlinearity, chalcogenide glass is also transparent in the midinfrared (mid-IR), and thus a laser design similar to the one presented here could be used for the fabrication of mid-IR lasers. For example, the chalcogenide fiber could be used not only for NPR, but also as a gain medium via four-wave mixing or the Raman effect. Another option consists of doping the chalcogenide glass (e.g., $Cr^{2+}/Fe^{2+}/Tb^{3+}$) to provide gain [10,11]. Such a compact laser source could be used in applications including spectroscopy [12], sensing [13], or Raman amplification and low-coherence interferometry in the noiselike pulse regime [8].

Figure 1 shows a schematic of the fiber ring laser. It comprises an erbium-doped fiber amplifier (EDFA), a segment of As_2S_3 fiber, two polarization controllers (PCs), and a polarizer. A coupler O_1 extracts 1% of the power out of the loop for monitoring purposes. The As_2S_3 fiber has a length $L_c = 19.5$ cm with a fiber nonlinear parameter $\gamma = 0.16\ \mathrm{W^{-1}m^{-1}}$, a material dispersion coefficient $\beta_{2,\mathrm{AsS}} = -522\ \mathrm{ps^{-1}/km}$, and a numerical aperture NA = 0.23. NPR takes place in that short segment of fiber having a γ parameter ~1000 times that of standard silica fiber. The As_2S_3 fiber is pigtailed to standard silica fibers using UV-cured epoxy, with a total insertion loss of 4.5 dB due to Fresnel reflection and mode mismatch. However, the mode mismatch could be completely eliminated with an appropriate adjustment of chalcogenide fiber core radius. In this case, it is expected that the insertion loss could be reduced down to the Fresnel losses, that is, 0.54 dB from $n_{\mathrm{AsS}} = 2.4$.

The EDFA is composed of ~10 m of erbium-doped fiber, with a material dispersion coefficient $\beta_{2,\mathrm{edfa}} = 5\ \mathrm{ps^2/km}$. The EDFA has a built-in isolator that conveniently ensures self-starting of the laser cavity [6]. The PCs are adjusted until self-pulsation occurs, in which case the round-trip losses for the continuous-wave (CW) light become higher than for the pulsed light. Figure 2 illustrates the mechanism of NPR along the pulse profile, which after passing through a polarizer leads to pulse shortening.

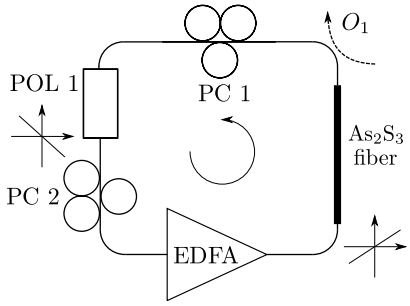

Fig. 1. Schematic of the As_2S_3 fiber ring laser and its polarization states.

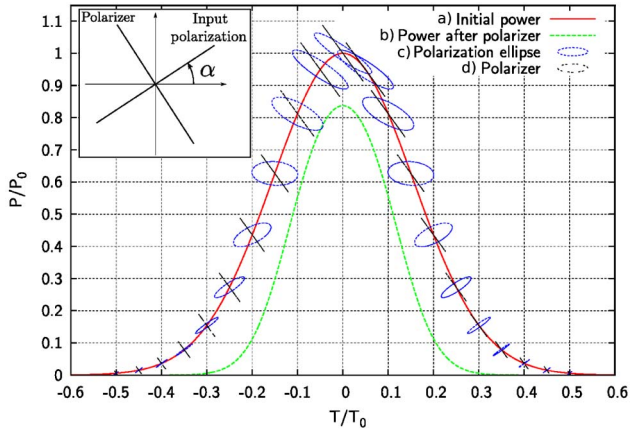

Fig. 2. (Color online) Illustration of the mechanism of NPR and filtering by the polarizer. (a) Initial power profile with linear polarization at angle α. (b) Power through polarizer. (c) Polarization state along the pulse profile, after NPR. (d) Polarization axis of the polarizer at angle $\alpha + \pi/2$.

A proper adjustment of the PCs leads to self-pulsation, spawned by NPR. The repetition rate of the laser is 10.42 MHz, which corresponds to a cavity length $L_1 = 19.9$ m. Two different regimes are observed, each with its own spectral and temporal properties. The first regime has a typical solitonic spectral shape including sidebands, typical of fiber lasers with average anomalous dispersion, and will be referred to as the solitonic regime. Appearing with a different PC adjustment, the second regime has a wider and flatter spectrum, without sidebands.

Figure 3 shows the spectrum in the solitonic regime, centered at a wavelength of 1560 nm. Sharp sidebands are present, as a consequence of the spectrum superposition between solitons and dispersive waves. Sudden variations of both the dispersion coefficient and the nonlinearity, as well as sudden variations of the pulse power due to an imperfect coupling, prevent the soliton from adapting adiabatically [14]. Apart from the peak at 1558 nm which corresponds to a copropagating CW signal, the sidebands are relatively strong [15]. This is a good indication that the minimal pulse width has been reached, itself determined by a small average anomalous

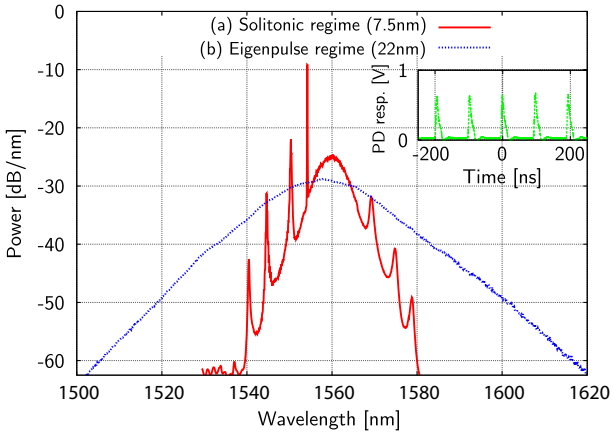

Fig. 3. (Color online) (a) Fiber laser spectrum operating in a solitonic regime. (b) Operation in a regime of noiselike pulses. Subplot: photodiode response at output O_1.

dispersion in the cavity. Linearly chirped 1 ps long pulses with an energy of $E_s = 37$ pJ are measured with the frequency resolved optical gating device. With sufficient dispersion compensation, the pulses could be recompressed down to 340 fs, while leaving no residual chirp.

From the spectrum of Fig. 3, both the average second- and third-order dispersion terms can be inferred. According to [4], the Nth sideband position in a solitonic regime is determined by the dispersion terms β_2 and β_3, the pulse width τ, the cavity length L, and the frequency offset to the central pulse wavelength $\Delta\omega$:

$$N = -\frac{L\beta_2}{4\pi}\left[\Delta\omega_N^2 + \frac{4\ln^2\left(1+\sqrt{2}\right)}{\tau_0^2}\right] - \frac{L\beta_3}{12}\Delta\omega_N^3. \quad (1)$$

By solving Eq. (1) for each discernible N, the optimal parameters for the second- and third-order dispersion, plus the pulse width, are calculated using a nonlinear conjugate gradient algorithm. Applied to this setup, we obtain $\tau = 326$ fs, $\langle\beta_{2,\mathrm{AsS+silica}}\rangle = -7.6$ ps^2/km, and $\beta_3 = 0.03$ ps^3/km. Figure 4 compares the experimental results with the best fit obtained out of Eq. (1). It must be pointed out that a more accurate value of β_3 could be obtained by making a fit of several measurements with varying cavity lengths.

Moreover, the information carried by the sidebands can be exploited by comparison with a similar setup, except for the absence of the chalcogenide fiber. The average second-order dispersion term is readily obtained for that second cavity, and takes into account the dispersion in the EDFA, and in the silica fiber segments for a total of $\langle\beta_{2,\mathrm{silica}}\rangle = -12.80$ ps^2/km. From Eq. (2), it is therefore straightforward to derive an expression for the second-order dispersion of the As_2S_3 fiber:

$$\langle\beta_{2,\mathrm{silica}}\rangle L_2 + \langle\beta_{2,\mathrm{AsS}}\rangle L_c = \langle\beta_{2,\mathrm{AsS+silica}}\rangle L_1 \quad (2)$$

with $L_2 = 19.7$ m the cavity length of the second cavity. In agreement with the expected values [16], we evaluated $\langle\beta_{2,\mathrm{AsS}}\rangle = 517.3$ ps^2/km.

The noiselike pulse regime provides a wide spectrum that stretches with respect to the PC tuning, as shown by the dotted line of Fig. 3. As can be observed on the

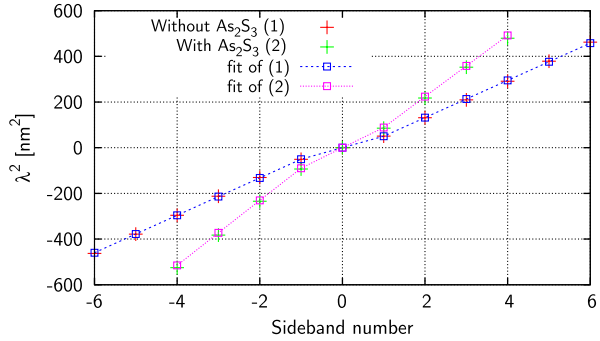

Fig. 4. (Color online) Sideband positions for both cavities. The second-order dispersion basically determines the slope of the squared wavelength offset to the pulse center. The small discrepancy visible at the first sidebands is due to the relatively short pulse duration τ_0 of Eq. (1).

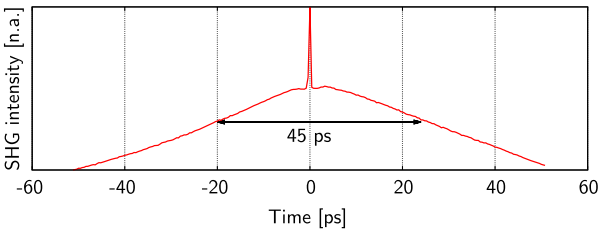

Fig. 5. (Color online) Autocorrelation of noiselike pulses.

autocorrelation trace for this regime on Fig. 5, no structured pulse can be retrieved from that regime, but rather noise at a femtosecond scale inside a picosecond envelope [17]. The temporal envelope of these noiselike pulses is of 45 ps.

The large bandwidth observed is a consequence of this pulse pattern, while its smooth profile is due to the fact that the spectrum analyzer performs an averaging over many spectra of these noiselike pulses. The origins of this regime are still unclear [17]. However, the relatively high energy $E_n = 3$ nJ of these noiselike pulses is interesting in comparison with Q-switching. Noiselike pulses are present at the repetition rate of the cavity, while Q-switched pulses usually have a less stable and lower repetition rate.

Passive mode-locking via NPR was achieved in a chalcogenide fiber, leading to picosecond chirped pulses. Two different regimes could be observed. As expected in anomalous dispersion, a solitonic regime with sidebands was observed, providing information about the average dispersion in the cavity [4].

In this work, we use the information carried by these sidebands to derive an accurate value of the material dispersion coefficient $\langle \beta_{2,\mathrm{AsS}} \rangle$ in the chalcogenide fiber. Because of the low level of dispersion involved, this can hardly be achieved with other methods that require significant power levels or require the single-mode condition [18,19]. We note that the high normal dispersion of As_2S_3 compensates by 40% the average dispersion provided by the silica fiber portion of the ring cavity. Further optimization of the cavity by reduction of the silica fiber will lead to shorter pulses.

The authors gratefully thank the National Optics Institute (Qc) for their financial support and Pierre Galarneau for constructive comments.

References

1. V. Matsas, T. Newson, D. Richardson, and D. Payne, Electron. Lett. **28**, 1391 (1992).
2. L. Nelson, D. Jones, K. Tamura, H. Haus, and E. Ippen, Appl. Phys. B **65**, 277 (1997).
3. R. Stolen, J. Botineau, and A. Ashkin, Opt. Lett. **7**, 512 (1982).
4. M. L. Dennis and I. N. Duling, III, IEEE J. Quantum Electron. **30**, 1469 (1994).
5. K. Tamura, E. Ippen, H. Haus, and L. Nelson, Opt. Lett. **18**, 1080 (1993).
6. H. Haus, E. Ippen, and K. Tamura, IEEE J. Quantum Electron. **30**, 200 (1994).
7. G. Sucha, D. Chemla, and S. Bolton, J. Opt. Soc. Am. B **15**, 2847 (1998).
8. M. Horowitz, Y. Barad, and Y. Silberberg, Opt. Lett. **22**, 799 (1997).
9. T. Schweizer, B. Samson, R. Moore, D. Hewak, and D. Payne, Electron. Lett. **33**, 414 (1997).
10. J. Sanghera, L. B. Shaw, and I. Aggarwal, IEEE J. Sel. Top. Quantum Electron. **15**, 114 (2009).
11. S. Mirov, V. Fedorov, I. Moskalev, D. Martyshkin, and C. Kim, Laser Photon. Rev. **4**, 21 (2010).
12. F. Tittel, D. Richter, and A. Fried, in *Solid-State Mid-Infrared Laser Sources* (2003), pp. 458–529.
13. U. Willer, M. Saraji, A. Khorsandi, P. Geiser, and W. Schade, Opt. Lasers Eng. **44**, 699 (2006).
14. H. Haus, K. Tamura, L. Nelson, and E. Ippen, IEEE J. Quantum Electron. **31**, 591 (1995).
15. M. Fermann, M. Andrejco, M. Stock, Y. Silberberg, and A. Weiner, Appl. Phys. Lett. **62**, 910 (1993).
16. C. Xiong, E. Magi, F. Luan, A. Tuniz, S. Dekker, J. Sanghera, L. Shaw, I. Aggarwal, and B. Eggleton, Appl. Opt. **48**, 5467 (2009).
17. S. Kobtsev, S. Kukarin, S. Smirnov, S. Turitsyn, and A. Latkin, Opt. Express **17**, 20707 (2009).
18. H. Shang, Electron. Lett. **17**, 603 (1981).
19. J. Lee and D. Kim, Opt. Express **14**, 11608 (2006).